

See discussions, stats, and author profiles for this publication at: <https://www.researchgate.net/publication/6705267>

# Structure of Poly(acrylic acid) in Electrolyte Solutions Determined from Simulations and Viscosity Measurements

ARTICLE *in* THE JOURNAL OF PHYSICAL CHEMISTRY B · DECEMBER 2006

Impact Factor: 3.3 · DOI: 10.1021/jp063981w · Source: PubMed

CITATIONS

43

READS

48

5 AUTHORS, INCLUDING:



**Zbigniew Adamczyk**

Akademickie Centrum Komputerowe CYFRO...

177 PUBLICATIONS 3,709 CITATIONS

SEE PROFILE



**Barbara Jachimska**

Polish Academy of Sciences

38 PUBLICATIONS 623 CITATIONS

SEE PROFILE



**Piotr Warszyński**

Instytut Katalizy i Fizykochemii Powierzchni i...

144 PUBLICATIONS 2,470 CITATIONS

SEE PROFILE

# Structure of Poly(acrylic acid) in Electrolyte Solutions Determined from Simulations and Viscosity Measurements

Z. Adamczyk,\* A. Bratek, B. Jachimska, T. Jasiński, and P. Warszyński

*Institute of Catalysis and Surface Chemistry Polish Academy of Science, Niezapominajek 8, 30-239 Cracow, Poland*

*Received: June 26, 2006; In Final Form: September 1, 2006*

In this work, the structure of poly(acrylic acid) (PAA) molecules in electrolyte solutions obtained from molecular dynamic simulations was compared with experimental data derived from dynamic light scattering (PCS), dynamic viscosity, and electrophoretic measurements. Simulations and measurements were carried out for polymer having a molecular weight of 12 kD for various ionic strengths of the supporting electrolyte (NaCl). The effect of the ionization degree of the polymer, regulated by the change in the pH of the solution in the range 4–9 units, was also studied systematically. It was predicted from theoretical simulations that, for low electrolyte concentration ( $10^{-3}$  M) and pH = 9 (full nominal ionization of PAA), the molecule assumed the shape of a flexible rod having the effective length  $L_{\text{ef}} = 21$  nm, compared to the contour length  $L_{\text{ext}} = 41$  nm predicted for a fully extended polymer chain. For an electrolyte concentration of 0.15 M, it was predicted that  $L_{\text{ef}} = 10.5$  nm. For a lower ionization degree, a significant folding of the molecule was predicted, which assumed the shape of a sphere having the radius of 2 nm. These theoretical predictions were compared with PCS experimental measurements of the diffusion coefficient of the molecule, which allowed one to calculate its hydrodynamic radius  $R_{\text{H}}$ . It was found that  $R_{\text{H}}$  varied between 6.6 nm for low ionic strength (pH = 9) and 5.8 nm for higher ionic strength (pH = 4). The  $R_{\text{H}}$  values for pH = 9 were in a good agreement with theoretical predictions of particle shape, approximated by prolate spheroids, bent to various forms. On the other hand, a significant deviation from the theoretical shape predictions occurring at pH = 4 was interpreted in terms of the chain hydration effect neglected in simulations. To obtain additional shape information, the dynamic viscosity of polyelectrolyte solutions was measured using a capillary viscometer. It was found that, after considering the correction for hydration, the experimental results were in a good agreement with the Brenner's viscosity theory for prolate spheroid suspensions. The effective lengths derived from viscosity measurements using this theory were in good agreement with values predicted from the molecular dynamic simulations.

## I. Introduction

Polyelectrolytes or polyions are molecules composed of a large number of covalently linked ionizable subunits. They are abundant in nature and essential for biological systems, including DNA. Polyelectrolytes are often used in pharmaceutical, cosmetic, and food industries, in ternary oil recovery, and for regulating rheological properties of suspensions.

Another important field of polyelectrolyte applications is preparing multilayer films on solid substrates of a desired composition and functionality,<sup>1–6</sup> which is often realized by layer-by-layer (LbL) deposition of anionic and cationic polyelectrolytes. The simplicity of this procedure, the feasibility of embedding various molecules, proteins, and colloid particles into the polymeric layer, opens a broad spectrum of possibilities to produce films of targeted architecture. A controlled formation of polymeric film requires a thorough knowledge of the structure of the polyelectrolyte molecules in relation to its molecular weight, ionic strength, and pH of the solutions.

One of the efficient ways of learning about structural aspects of polyelectrolytes are the rheological measurements, which have been performed extensively over the decades.<sup>7–13</sup> Because of the variety of parameters critically influencing the viscosity, especially in the range of low electrolyte concentration, the

otherwise valuable results are often misinterpreted. The main source of discrepancies is the assumption of the salt-free solutions. Even in the totally deionized water, the residual concentration of ions must be higher than  $2 \times 10^{-7}$  M (at neutral pH = 7). Because of carbon dioxide dissolution, this is normally increased to  $\sim 10^{-5}$  M, if the measurement atmosphere is not controlled. Moreover, adding charged molecules into the solution simultaneously introduces counterions, whose concentration is dependent on the polyelectrolyte ionization (dissociation) degree, which depends in turn on the pH and ion composition.

With increasing concentration, many-body effects appear, because of hydrodynamic, electrostatic, and other specific interactions between macromolecule chains. This makes the entire problem nonlinear in respect to the polyelectrolyte concentration, making the interpretation of the viscosity data rather involved.

On the other hand, adsorption of polyelectrolytes on the walls of containers (capillaries) creates problems for the range of very low concentrations. This may often lead to the appearance of the maxima on the intrinsic viscosity vs concentration dependence.<sup>8,9</sup>

Macromolecule aggregates forming in unfiltered solution introduce additional problems because they may break up with increasing shear rate, leading to apparent non-Newtonian behavior, interpreted as the shear-thinning processes.

\* To whom correspondence should be addressed.

All these complications and the variety of controlling parameters makes a theoretical description of polyelectrolyte viscosity a vastly complicated task. As a result, none of existing theoretical approaches are general enough to fully account for experimentally observed data.

One of the first approaches was the scaling theory of de Gennes et al.,<sup>14</sup> predicting the configuration of flexible polyelectrolytes in solutions with no added salt.

A considerable fraction of recent theoretical works is based on the concept of the electrostatic wormlike chain theory developed by Odjik<sup>15</sup> and Skolnick and Fixman,<sup>16</sup> known as the Odjik–Skolnick–Fixman (OSF) theory. This approach was based on the persistence length  $L_p$  concept, whose electrostatic contribution was calculated by solving the linearized Poisson–Boltzmann equation for a uniform line charge. It was predicted that, because of electrostatic repulsion, this electrostatic component of  $L_p$  increases proportional to the square of Debye screening length  $\kappa^{-1}$ , i.e., inversely proportionally to the ionic strength,  $I$ , of polyelectrolyte solution. The persistence length expression has been corrected by Davis and Russel,<sup>17</sup> who calculated the correction valid for arbitrary  $\kappa d_e$  (where  $d_e$  is the polymer chain diameter).

By exploiting the concept of the persistence length, Yamakawa and Fujii<sup>18</sup> formulated a viscosity theory for the wormlike polymers, which predicts that the intrinsic viscosity increases proportionally to  $L_p^{3/2}$ , i.e., proportionally to the cube of the Debye screening length. The OSF theory and the Yamakawa–Fujii model was modified by Rushing and Hester,<sup>12</sup> who proposed a semiempirical model, which correlated the intrinsic viscosity of polyelectrolytes with its molecular weight and the screening length in the limit of high electrolyte concentration. They found, by extensively analyzing existing experimental data for various polyelectrolytes, that the slope of the intrinsic viscosity vs the screening length dependence was 1.62 rather than 3.

The wormlike model was modified by Davis and Russel,<sup>19</sup> who considered the excluded volume effect, which introduced additional stiffness of the polymer chain, characterized in terms of the chain expansion factor. This allowed them to renormalize the persistence length occurring in the Yamakawa–Fujii model and properly reflect the effect of the molecular weight and the ionic strength on the intrinsic viscosity for potassium poly(styrene sulfonate) solutions.

The dynamic viscosity data for the wormlike regime can be quantitatively interpreted in terms of the hydrodynamic model proposed originally by Kirkwood and Auer,<sup>20</sup> who assumed an extended, rodlike shape of polyelectrolytes. In the more general case of ellipsoidal or spheroidal shape of macromolecules, one can use the well-established results of Brenner<sup>21</sup> and Harding,<sup>22</sup> who derived analytical solutions for the intrinsic viscosity as a function of the axis ratio parameters. However, these theoretical results can only be applied if the shape of the molecule is known as a function of various physicochemical parameters.

On the basis of this analysis, it seems rather improbable that a universal theory of polyelectrolyte solutions will emerge in the future that simultaneously predicts the shape of the polyelectrolyte and the dynamic viscosity over a broad range of concentrations.

Because of the lack of such a universal theory, a true structure of polyelectrolytes in solutions cannot be unequivocally determined from viscosity measurements alone. Complementary data are necessary, such as the hydrodynamic radius of molecules (containing shape information), their electrophoretic mobility, enabling estimations of the true ion condensation degree, etc.

**TABLE 1: Physicochemical Characteristics of PAA,  $M_w = 12\,000$  and  $T = 293\text{ K}$**

characteristic	value, unit	remarks
density, $\rho_p$	$1.23 \times 10^3 \text{ kg}\cdot\text{m}^{-3}$	manufacturer
molecular weight	12 kD	manufacturer
molecular weight of monomer	72 D	calculated
number of monomers, $N_m$	167	calculated
bare chain diameter, $d_e$	0.71 nm	calculated
hydrated chain diameter $d_h$	1.0 nm	calculated
extended length, $L_{\text{ext}}$	40.9 nm	calculated
radius of gyration, $R_g$	11.8 nm	calculated
equivalent sphere radius, $R_s$	1.57 nm	calculated
volume of monomer	$9.7 \times 10^{-2} \text{ nm}^3$	calculated
volume of molecule	$16.2 \text{ nm}^3$	calculated
aspect ratio, $L_{\text{ext}}/d_h$	40.9	calculated

Additionally, the interpretation of experimental data can be facilitated by a comparison with theoretical simulations, based on the molecular dynamic approach, which furnish the necessary shape information.

Despite the major significance of such a complex approach, there are few systematic works in the literature combining theoretical simulations of molecular structure with experimental measurements of diffusion coefficients and viscosity.<sup>19</sup> Thus, the goal of this work is to develop such an approach aimed at a full analysis of the structure of poly(acrylic acid) (PAA), which is widely used as a model polyelectrolyte. This is so because of its simple chemical composition and possibility of regulating the ionization degree of the polymer, merely by the change in the pH.

## II. Materials and Methods

The polyelectrolyte used in our studies was the poly(acrylic acid) (PAA), kindly supplied by Coatex (France) of an anionic type, having an averaged molecular weight  $M_w = 12\text{ kD}$  and the density  $1.23 \times 10^3 \text{ kg}\cdot\text{m}^{-3}$  (determined by the manufacturer). Accordingly, the molecular volume of the polymer chain was  $v_e = M_w/\rho_p A_v$  (where  $A_v$  is the Avogadro number) =  $16.2 \text{ nm}^3$  (for sake of convenience, the relevant physicochemical data for the polymer are compiled in Table 1).

Doubly distilled water was used for the preparation of all solutions. Sodium chloride, HCl, and NaOH were commercial products of Aldrich and Sigma. NaCl was used as a background electrolyte. All electrolyte solutions were filtered using a  $0.22 \mu\text{m}$  Millipore filter. The temperature of the experiments was kept constant at  $293 \pm 0.1 \text{ K}$ .

The electrophoretic mobility and diffusion coefficient of the polyelectrolyte were determined using the Zetasizer Nano ZS of Malvern (measurements range of  $3\text{--}10 \mu\text{m}$  for zeta potential and  $0.6 \text{ nm--}6 \mu\text{m}$  for particle size). Zeta potentials were determined for ionic strength values (regulated by NaCl content) of  $I = 10^{-3} \text{ M}$ ,  $5 \times 10^{-3} \text{ M}$ ,  $10^{-2} \text{ M}$ , and  $0.15 \text{ M}$  and pH range  $2.0\text{--}9.0$ , whereas the diffusion coefficients were determined for the same ionic strength and pH equal to  $4.0$ ,  $5.5$ , and  $9.0$ , respectively.

The dynamic viscosities of polyelectrolyte solutions were measured using a capillary viscometer equipped with a conductivity sensor of solution level. The averaged shear rate  $\langle G \rangle$  in the capillary was  $1.8 \times 10^2 \text{ s}^{-1}$ .

The concentration of PAA solutions used in the viscosity measurements was changed within the range  $0.05\text{--}5 \text{ kg}\cdot\text{m}^{-3}$  ( $50\text{--}5000 \text{ ppm}$ ). The intrinsic viscosity was measured for three values of pH equal to  $4.0$ ,  $5.5$ , and  $9.0$  and four ionic strength values ( $I = 10^{-3} \text{ M}$ ,  $I = 5 \times 10^{-3} \text{ M}$ ,  $I = 10^{-2} \text{ M}$ , and  $I =$

0.15 M). The density of the polyelectrolyte solutions needed for viscosity evaluation was determined by a pycnometer.

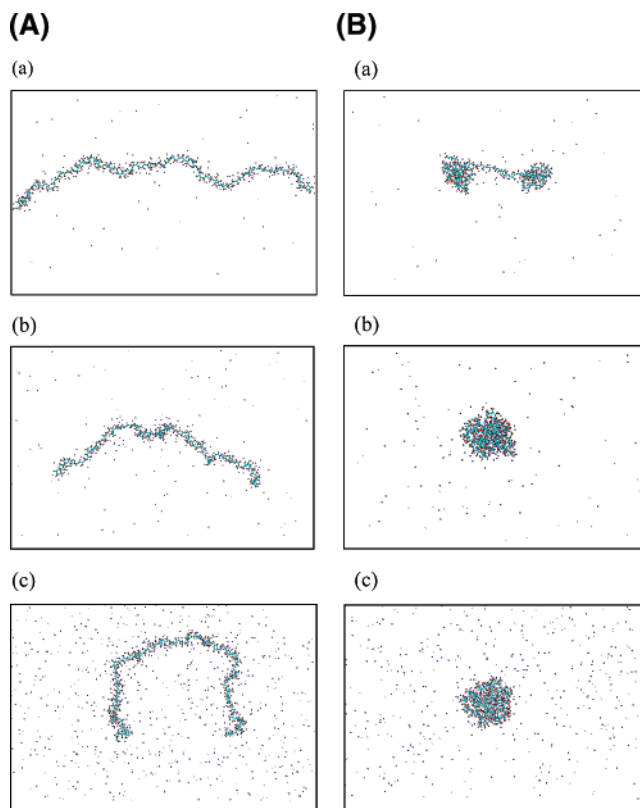
Calculations of polyelectrolyte structure were performed according to the molecular dynamic simulations using the HYPERCHEM 7.5 software package.<sup>23</sup> All calculations are performed using the AMBER 99<sup>24</sup> force field contained in the package with the polymer chains in the united atom representation. Partial atomic charges for polyelectrolyte ions were assigned according to the QSAR procedure<sup>25</sup> also contained in HYPERCHEM. The electrostatic interactions were calculated using the periodic box of dimensions  $300 \times 300 \times 300$  nm assuming the “primitive” model of electrolyte with explicit ions  $\text{Na}^+$  and  $\text{Cl}^-$  added to the box to achieve the required ionic strength of  $10^{-3}$  M,  $10^{-2}$  M, and 0.15 M. The aqueous solvent was treated as a continuous dielectric medium with the dielectric relative permittivity  $\epsilon = 80$ . The simulation procedure was as follows. First, the polyelectrolyte with the required degree of charged groups was constructed, and the partial atomic charges were assigned. Next, the polyelectrolyte molecule was inserted into the simulation box with the electrolyte ions. The molecular mechanics simulation was performed for ions only, at constant temperature 300 K, to obtain initial ion distribution along the chain. Then, the Langevin dynamics simulation (friction coefficient  $0.01 \text{ ps}^{-1}$ ) was performed until the equilibrium average conformation was reached, i.e., the average total energy of the system was constant. When the equilibrium was reached, the Langevin simulation was continued and randomly selected snapshots of polyelectrolyte molecule were taken. Because of the variable shape of PAA molecule found under various conditions, it was difficult to define unequivocally a characteristic linear dimension such as the end-to-end length or the radius of gyration. For sake of convenience, we have introduced here the effective length parameter  $L_{\text{ef}}$ , which can be a useful measure of molecule dimensions if it assumes an elongated shape. This parameter also facilitates the interpretation of dynamic viscosity measurements in terms of the hydrodynamic theory. The effective length was calculated as an averaged value of the distance between the surfaces of the two outermost atoms of the molecule averaged at the fluctuating equilibrium state. As condensed counterions, these ones with the distance to the polyelectrolyte of  $<1.1$  of the sum of van der Waals atomic radii were assumed.

### III. Results and Discussion

#### III.A. PAA Characteristics Derived from Simulations.

Theoretical simulations were carried out for the PAA having a molecular weight  $M_w$  of 12 kD. Since the monomer molecular weight is 72, the macromolecule consisted of 167 monomers. Accordingly, the maximum nominal charge of the molecule (assuming full ionization) was  $167 \times (1.6 \times 10^{-19}) \text{ C} = 2.67 \times 10^{-17} \text{ C}$ . Calculations described below were performed for molecule charge of  $2.67 \times 10^{-17} \text{ C}$  (167 nominal charges per molecule, 100% nominal ionization degree, denoted by  $\alpha$ ),  $1.33 \times 10^{-17} \text{ C}$  (83 charges, 50% ionization), and  $0.53 \times 10^{-17} \text{ C}$  (33 charges, 20% ionization) for ionic strengths of  $10^{-3}$  M,  $10^{-2}$  M, and 0.15 M, respectively. The calculations allowed one to determine the effective chain diameter, its shape, and the characteristic linear dimensions under various conditions, e.g., the effective length  $L_{\text{ef}}$  and the amount of mobile charges located outside the slip plane.

The equivalent van der Waals diameter of bare chain  $d_c$  obtained from our calculations was 0.71 (see Table 1). This is slightly larger than the unreduced polymer diameter equal to 0.6 nm, calculated previously.<sup>12</sup> Using this value of  $d_c$  and



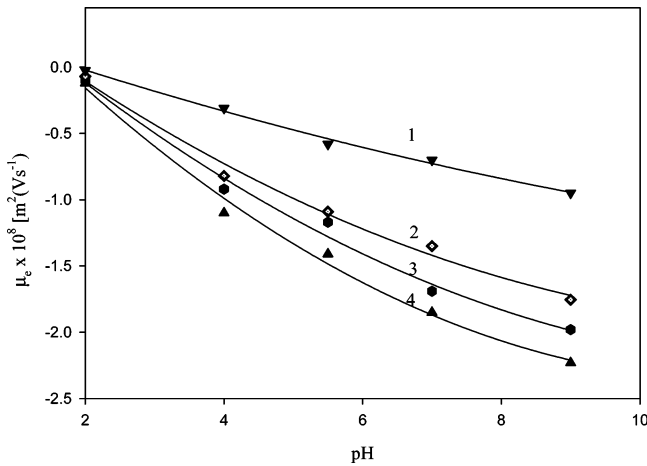
**Figure 1.** (A) Snapshots of PAA molecule conformations derived from numerical simulations, nominal ionization degree:  $\alpha_i = 1.0$ ; (a)  $-I = 10^{-3}$  M,  $L_{\text{ef}} = 21.0$  nm; (b)  $-I = 10^{-2}$  M,  $L_{\text{ef}} = 18.5$  nm; (c)  $-I = 10^{-1}$  M,  $L_{\text{ef}} = 10.5$  nm. (B) Snapshots of PAA molecule conformations derived from numerical simulations, nominal ionization degree:  $\alpha_i = 0.5$ ; (a)  $-I = 10^{-3}$  M,  $L_{\text{ef}} = 7.9$  nm; (b)  $-I = 10^{-2}$  M,  $L_{\text{ef}} = 4.0$  nm; (c)  $-I = 10^{-1}$  M,  $L_{\text{ef}} = 4.0$  nm.

previously found volume  $v_e$ , one can deduce that the extended length (often referred to as the contour length<sup>19</sup>) of the molecule  $L_{\text{ext}} = 4v_e/\pi d_c^2$  equals 40.9 nm (assuming its cylindrical shape). Another limiting dimension of the macromolecule is the equivalent sphere radius  $R_s = (3v_e/4\pi)^{1/3}$ , i.e., the radius of the sphere having the same volume as the polymer molecule, which was 1.57 nm in our case (see Table 1).

Snapshots of equilibrated PAA chain configurations shown in Figure 1 for the 100% ionization degree indicate that, for low ionic strength, the molecule assumes an extended, wormlike shape characterized by the effective length  $L_{\text{ef}} = 21$  nm (for  $10^{-3}$  M). For increasing ionic strength, the effective length is decreased because of the folding of the molecule, becoming 18.5 nm for  $I = 10^{-2}$  M and 10.5 nm for  $I = 0.15$  M. A similar behavior was predicted before in the simulations of Chodanowski and Stoll,<sup>26</sup> who studied theoretically configurational transitions in polyelectrolyte solution applying the Monte Carlo simulations.

For lower ionization degree  $\alpha = 0.5$ , the simulated shape of the molecule resembles a dumbbell (see Figure 2), as a result of a significant folding starting from the ends. The contour length of the dumbbell was found equal to 7.9 nm for  $10^{-3}$  M. For higher ionic strength, a random coil shape of the molecule was predicted (see Figure 2, parts b and c) having the diameter of 4 nm, which is slightly larger than the equivalent sphere diameter of 3.14 nm (see Table 1). It is worth it to mention that, in these simulations, the solvent (water) was not explicitly considered, so all the hydration effects were not accounted for. Therefore, the true shape of the molecule under various





**Figure 2.** Dependence of electrophoretic mobility of PAA  $\mu_e$  on pH determined experimentally: (1)  $I = 0.15$  M, (2)  $I = 10^{-2}$  M, (3)  $I = 5 \times 10^{-3}$  M, (4)  $I = 10^{-3}$  M.

conditions can only be determined by confronting the theoretical results with experimental measurements of the diffusion coefficient (hydrodynamic radius) and the intrinsic viscosity.

As discussed in refs 22 and 27, the diffusion coefficients (for translation and rotary motion) as well as intrinsic viscosity can be theoretically predicted in terms of the hydrodynamic model based on the creeping flow concept. It is so because flows associated with polyelectrolyte motion in solutions are characterized by very low Reynolds number  $Re = LV/\nu$  (where  $L$  is the characteristic length scale of the motion,  $V$  is the characteristic velocity, and  $\nu$  is the kinematic viscosity of the solution). It can be estimated by assuming  $L = L_{ext}/2 = 20$  nm that, in aqueous solutions ( $\nu = 10^{-6}$  m<sup>2</sup>/s,  $T = 293$  K),  $Re = 2 \times 10^{-2}$  for molecule translation velocity as large as 1 m/s. As a consequence of low  $Re$  number, the relaxation time of establishing the stationary conditions of the flow distribution around a moving polyelectrolyte molecule  $\tau_h = L^2/\nu$  remains very small. For the above values of  $L$  and  $\nu$ , the momentum relaxation time is  $4 \times 10^{-10}$  s.

For comparison, the diffusion relaxation time can be estimated from the formula

$$\tau_d = L^2/D \quad (1)$$

where  $D = kT/6\pi\eta R_H$  is the characteristic translation diffusion coefficient of the polymer ( $k$  is the Boltzmann constant,  $\eta$  is the dynamic viscosity of the solvent, and  $R_H$  is the hydrodynamic radius of the polymer). Assuming  $R_H = 20$  nm and  $\eta = 10^{-3}$  kg/(ms)<sup>-1</sup>, one obtains  $\tau_d = 3.7 \times 10^{-5}$  s, which is almost 5 orders of magnitude larger than the momentum relaxation time. This estimation shows that, because of rapid momentum relaxation in comparison with diffusion, the fluid velocity field adjusts instantaneously to the polyelectrolyte molecule motion. As a consequence, the hydrodynamic resistance coefficient can be evaluated by considering the real geometrical shape of the molecule rather than the space-averaged shape characterized, e.g., by the radius of gyration.

It seems reasonable, in our case, to approximate the behavior of PAA molecules in electrolyte solutions by a particle having a spheroidal shape. For spheroids, as well as for similar bodies possessing a before and after symmetry, e.g., cylinders, bent spheroids, disks, rings, etc., the translation and rotation diffusion matrices assume the form<sup>27,28</sup>

$$\mathbf{D} = kT \quad \mathbf{M} = \frac{kT}{\eta} \begin{vmatrix} 1/K_{||} & 0 \\ 0 & 1/K_{\perp} \\ 0 & 1/K_{\perp} \end{vmatrix} \quad (2)$$

$$\mathbf{D}_r = kT \quad \mathbf{M}_r = \frac{kT}{\eta} \begin{vmatrix} 1/K_{||} & 0 \\ 0 & 1/K_{r_{\perp}} \\ 0 & 1/K_{\perp} \end{vmatrix}$$

where  $\mathbf{M}$  and  $\mathbf{M}_r$  are the translation and rotation mobility matrices,  $K_{||}$  and  $K_{\perp}$  are the hydrodynamic resistance coefficients for the translation motion along the symmetry axes, and  $K_{||}$  and  $K_{r_{\perp}}$  are the coefficients for the rotary motion.

The averaged translation diffusion coefficient (scalar), which can be determined experimentally by, e.g., the dynamic light scattering, is given by<sup>28,29</sup>

$$\langle D \rangle = \frac{kT}{3\eta} \left( \frac{1}{K_{||}} + \frac{2}{K_{\perp}} \right) = \frac{kT}{6\pi\eta R_H} \quad (3)$$

where the quantity

$$R_H = \frac{1}{2\pi} \left( \frac{1}{K_{||}} + \frac{2}{K_{\perp}} \right) \quad (4)$$

is usually defined as the hydrodynamic radius of the body (for translational motion)

The coefficients  $K_{||}$ ,  $K_{\perp}$ ,  $K_{r_{||}}$ ,  $K_{r_{\perp}}$ , and  $R_H$  are known in analytical form for prolate and oblate spheroids. They are explicitly given by<sup>21</sup>

$$\begin{aligned} K_{||} &= \frac{16\pi a}{\lambda^2(2\beta + \alpha_{||})} & K_{\perp} &= \frac{16\pi a}{2\lambda^2\beta + \alpha_{\perp}} \\ K_{r_{||}} &= \frac{2}{3\alpha_{\perp}} \nu_s & K_{r_{\perp}} &= \frac{2(\lambda^2 + 1)}{3(\lambda^2\alpha_{||} + \alpha_{\perp})} \nu_s \\ R_H &= \frac{a}{\lambda^2\beta} \end{aligned} \quad (5)$$

$$\alpha_{||}(\lambda) = \frac{2}{\lambda^2 - 1} (\lambda^2\beta - 1) \quad \alpha_{\perp}(\lambda) = \frac{\lambda^2}{\lambda^2 - 1} (1 - \beta) \quad (6)$$

$$\beta = \frac{\cos^{-1} \lambda}{\lambda(1 - \lambda^2)^{1/2}} \quad \beta = \frac{\cosh^{-1} \lambda}{\lambda(\lambda^2 - 1)^{1/2}} = \frac{\ln[\lambda + (\lambda^2 - 1)^{1/2}]}{\lambda(\lambda^2 - 1)^{1/2}}$$

oblate spheroids prolate spheroids (7)

where  $a$  and  $b$  are the semiaxes of the spheroid,  $\nu_s$  is the volume of the spheroid equal to  $(4/3)\pi ab^2$  for prolate and  $(4/3)\pi a^2b$  for oblate spheroids, for oblate spheroids  $\lambda = b/a < 1$ , and for prolate spheroids  $\lambda = a/b > 1$ .

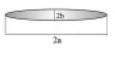



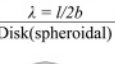
Interesting limiting forms can be derived from the above equations for prolate spheroids when  $\lambda \gg 1$  (slender bodies limit). In this case, the expression for the hydrodynamic radius becomes

$$R_H = \frac{a}{(c_1 \ln 2\lambda - c_2)} \quad (8)$$

where, for spheroids,  $c_1 = 1$  and  $c_2 = 0$ .

It was shown that eq 8 applies for other slender bodies<sup>27</sup> with the coefficients  $c_1 = 1$ ,  $c_2 = 0.11$  for cylinders (rods);  $c_1 = 11/12$ ,  $c_2 = 0.31$  for bent spheroids forming a semicircle

**TABLE 2: Analytical and Approximate Expressions for  $R_H$  and  $[\eta]$  for Particles of Various Shape**

Particle shape	$R_H$ [exact]	$R_H$ [approximate] $\lambda \gg 1$	$[\eta]$ approximate
Prolate spheroid  $\lambda = a/b$	$a \frac{(\lambda^2 - 1)^{1/2}}{\cosh^{-1} \lambda}$	$\frac{a}{\ln 2\lambda}$	$\frac{\lambda^2}{15} \left[ \frac{3}{\ln 2\lambda - 0.5} + \frac{1}{\ln 2\lambda - 1.5} \right] + \frac{8}{5}$
Cylinder  $\lambda = a/b$	-	$\frac{a}{\ln 2\lambda - 0.11}$	$\frac{\lambda^2}{15} \left[ \frac{3}{\ln 2\lambda - 0.5} + \frac{1}{\ln 2\lambda - 1.5} \right] + \frac{14}{15}$
Bent spheroid  $\lambda = l/2b$	-	$\frac{l}{2 \left[ \frac{11}{12} \ln 2\lambda - 0.31 \right]}$	-
Torus  $\lambda = l/2b$	-	$\frac{l}{2 \left[ \frac{11}{12} \ln 2\lambda - 1.20 \right]}$	-
Disk(spheroidal)  $\lambda = b/a$	$\frac{a(1 - \lambda^2)^{1/2}}{\cos^{-1} \lambda}$	$\lambda \rightarrow 0$ $\frac{2}{\pi} a$	-

(semitorus); and  $c_1 = 11/12$ ,  $c_2 = 1.20$  for spheroids bent to the form of a torus (ring).

It can also be noticed from eq 8 that the hydrodynamic radius increases for  $\lambda \gg 1$  proportionally to  $a/[\ln(2a/b)]$ , which is a function rather insensitive to the particle linear dimension (effective length of the polyelectrolyte molecule).

Analogously, the perpendicular rotary diffusion coefficient in the limit of  $a/b \gg 1$  (prolate spheroids) is given by the expression

$$D_{r_{\perp}} = \frac{kT}{8\pi\eta R_{H_r}^3} \quad (9)$$

where

$$R_{H_r} = a \left[ \frac{2}{3} \frac{(1 + 1/\lambda^2)}{(\lambda^2 \alpha_{\parallel} + \alpha_{\perp})} \right]^{1/3} \quad (10)$$

is the hydrodynamic radius for the rotary motion.



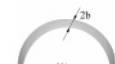



For  $\lambda \gg 1$ , eq 10 simplifies to

$$R_{H_r} = a \{3[\ln(2\lambda) - 0.5]\}^{-1/3} \quad (11)$$

In Table 2, the expressions for calculating the hydrodynamic radius of molecules of various shape are collected.

As can be noticed from the above formula, no adjustable parameters are needed to calculate the hydrodynamic radius. Therefore, it can be used in our case for the PAA molecule, by considering that  $L_{\text{ext}} = 40.9$  nm. Another parameter which is needed is the aspect ratio  $\lambda = L_{\text{ext}}/d_h$ , where  $d_h$  is the hydrated chain diameter. It can be postulated that this corresponds to the geometrical diameter  $d_e$  plus one layer of water dipoles,<sup>22</sup> having the size of 0.145 nm. This gives  $d_h = 1$  nm and  $\lambda = 40.9$ . Values

**TABLE 3: Values of the Hydrodynamic Radius  $R_H$  and Diffusion Coefficient Predicted for Various PAA Molecule Shapes**

Assumed molecule shape	$R_H$ [nm]	$D$ [ $\text{m}^2 \text{s}^{-1}$ ]	$D_r$ [ $\text{s}^{-1}$ ]	$[\eta]$
Prolate spheroids 	4.64	$4.62 \times 10^{-11}$	$2.2 \times 10^5$	126
Cylinder 	4.76	$4.51 \times 10^{-11}$		126
Bent spheroid 	5.49	$3.91 \times 10^{-11}$		
Torus (ring) 	7.21	$2.98 \times 10^{-11}$		
Disk (spheroidal) 	4.14	$5.18 \times 10^{-11}$		
Equivalent sphere 	1.57 (1.72)*	$1.37 \times 10^{-10}$	$4.16 \times 10^7$	2.5

\*Hydrated sphere radius.

of  $R_H$  calculated from eq 8 using these parameters for various postulated shapes of PAA molecule are collected in Table 3. One can notice that  $R_H = 4.6$  nm for a prolate spheroid, which is the smallest value of all configurations. For a cylindrical particle of the same aspect ratio,  $R_H = 4.8$  nm. Bending of the molecule increases  $R_H$  (and proportionally the hydrodynamic resistance coefficient), which attains 7.2 nm for the toroidal shape. Thus, contrary to intuition, deformation of macromolecules is expected to increase its hydrodynamic radius, i.e., decrease the diffusion coefficient. Interestingly enough, the hydrodynamic radius of a circular ring having the same size as the torus ( $L_{\text{ext}}/2\pi$ ) is much smaller and equal to 4.14 nm.

On the other hand, the hydrodynamic radius corresponding to rotary diffusion, calculated from eqs 9 and 10, equals 9 nm, which gives  $D_{r_{\perp}} = 2.2 \times 10^5 \text{ s}^{-1}$ . The rotary diffusion coefficient is an important parameter because it allows one to determine the range of validity of various rheological regimes of polyelectrolyte suspensions. This can be done by introducing the rotary Peclet number representing the ratio of the convective rotary motion due to shear flow to rotary diffusion motion. Accordingly, the  $Pe$  number is defined as<sup>21,29</sup>

$$Pe = \frac{\langle G \rangle}{D_{r_{\perp}}} \quad (12)$$

where  $\langle G \rangle$  is the averaged fluid velocity gradient of the shear flow.

If  $Pe \ll 1$ , the rotary diffusion dominates over the flow, so there is practically no molecule alignment in the flow direction, and all their orientations are accessible with equal probability.

Under such conditions, one can specify analytical formulas describing the intrinsic viscosity of suspension of spheroidal particles. The intrinsic viscosity  $[\eta]$  is defined as the slope of the dependence of  $\eta_s/\eta$  on the volume fraction of the solid in the suspension  $\Phi_s$  (where  $\eta_s$  is the suspension viscosity and  $\eta$  is the solvent viscosity).<sup>21</sup>

In the case of spheroidal particles immersed in simple shear flows, Brenner<sup>21</sup> has shown that the intrinsic viscosity is described by the general expression

$$[\eta] = 5Q_1(\lambda) - Q_2(\lambda) + 2Q_3(\lambda) = F_v(\lambda) \quad (13)$$

where

$$\begin{aligned} Q_1 &= \frac{1}{5\alpha'_{||}} \\ Q_2 &= \frac{2}{15\alpha'_{||}\left(1 - \frac{\alpha''_{||}}{\alpha'_{\perp}}\right)} \\ Q_3 &= \frac{1}{5\alpha'_{||}} \left[ \frac{\lambda(\alpha_{||} + \alpha_{\perp})(\alpha'_{||})}{\lambda^2\alpha_{||} + \alpha_{\perp}} \left( \frac{\alpha'_{||}}{\alpha'_{\perp}} \right) - 1 \right] \\ \alpha'_{||} &= \frac{\lambda^2}{4(\lambda^2 - 1)^2} (3\beta + 2\lambda^2 - 5) \\ \alpha''_{||} &= \frac{\lambda^2}{4(\lambda^2 - 1)^2} [2\lambda^2 + 1 - (4\lambda^2 - 1)\beta] \\ \alpha'_{\perp} &= \frac{\lambda}{(\lambda^2 - 1)^2} (\lambda^2 - 3\lambda^2\beta + 2) \\ \alpha''_{\perp} &= \frac{\lambda^2}{(\lambda^2 - 1)^2} \left[ \left( \frac{2\lambda^2 + 1}{\beta} \right) - 3 \right] \end{aligned} \quad (14)$$

For prolate spheroids, in the limit of  $a \gg b$ , eqs 13 and 14 reduce to the simpler form

$$[\eta] = \frac{\lambda^2}{15} \left[ \frac{3}{\ln 2\lambda - 0.5} + \frac{1}{\ln 2\lambda - 1.5} \right] + \frac{8}{5} \quad (15)$$

It is interesting to observe that the intrinsic viscosity of prolate spheroids in the limit  $\lambda \gg 1$  is more sensitive to the length of the body than the hydrodynamic radius  $R_H$ , because it increases proportionally to  $a^2/[\ln(2a/b)]$ .

In the case of PAA suspensions by substituting  $\lambda = 40.9$ , one obtains from eq 15  $[\eta] = 126$ , which is the maximum value of intrinsic viscosity for any physicochemical conditions.

**III.B. Comparison with Experimental Results.** The hydrodynamic radius determined by dynamic light scattering (PCS) for PAA was 6.6 nm (polymer concentration 250 ppm, pH = 9, and ionic strength  $10^{-3}$  M). This is close to the averaged value of  $R_H = 6.35$  nm for a spheroid of the length 40.9 nm bent to the form of semicircle and a torus (see Table 3). With increasing ionic strength, the value of  $R_H$  increased, becoming 8.1 nm for  $I = 0.15$ . This is close to the  $R_H$  value of 7.2 nm predicted for the torus (circular ring). This finding, which is in accordance with the simulated molecule shape (see Figure 1), suggests that the hydrodynamic model works reasonably well.

However, an unexpected behavior was observed for pH = 4, where the nominal ionization degree of PAA is expected to decrease significantly. The experimental  $R_H$  value at this pH and  $I = 10^{-3}$  M was 5.1 nm. For  $I = 0.15$  M (the same pH),

the measured  $R_H$  value was 5.8 nm. These observations suggest that the shape of the molecule is not changed too significantly with the increase in the ionic strength. This disagrees with the theoretical prediction of the molecule shape for lower ionization degree (see Figure 2), where a complete folding of the molecule is predicted, leading to a random coil structure, characterized by the  $R_H$  value of 2 nm.

One source of this discrepancy could be the finite concentration of the polymer solution necessary for hydrodynamic radius measurements, which was 250 ppm as mentioned above. For the semidilute regime of polyelectrolytes, there appear two effects, which influence the diffusion coefficient:<sup>28,30</sup>

(i) the increase in the hydrodynamic resistance coefficient due to the presence of adjacent molecules and

(ii) the increase in the chemical activity (potential) of the molecule due to steric interactions between chains.

For the semidilute regime, these corrections can be expressed as linear functions of the volume fraction of solid, in the following form.<sup>28,30</sup>

$$D = D^0(1 - C_1\Phi_V)(1 + 2B_2\Phi_V) = 1 + C_2\Phi_V \quad (16)$$

where  $D^0$  is the diffusion coefficient in the limit of infinite dilution,  $C_1$  is the dimensionless constant describing the hydrodynamic effects,  $\bar{B} = B_2/\nu_e$ ,  $B_2$  is the second virial coefficient, and  $\nu_e$  is the molecule volume,  $C_2 = 2B_2 - C_1$ .

Accordingly, the correction to the  $R_H$  is given by

$$R_H = R_H^0 \frac{D^0}{D} = R_H(1 - C_2\Phi_V) \quad (17)$$

where  $R_H^0$  is the hydrodynamic radius in the limit of infinite dilution.

The  $C_1$  constant for the long-time diffusion can be approximated by the expression<sup>22</sup>

$$C_1 = 1.6[\eta] \quad (18)$$

On the other hand, the reduced second virial coefficient for slender bodies, of the characteristic length  $L$ , can be approximated by

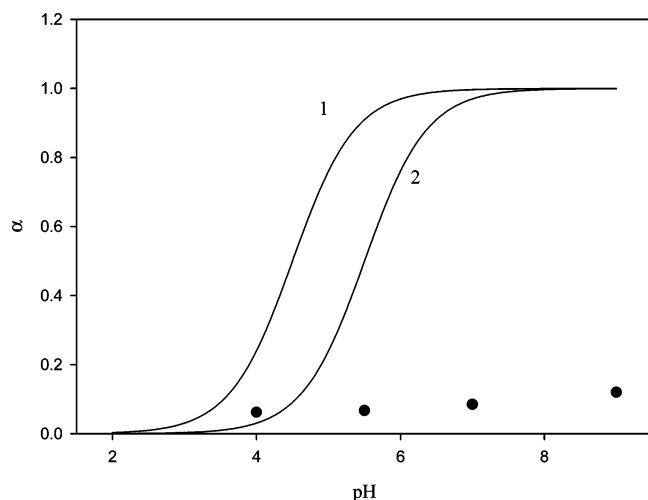
$$\bar{B}_2 = \frac{\pi L^3}{32\nu_m^*} \quad (19)$$

where  $\nu_m^*$  is the effective (hydrated) volume of the particle.

Thus, for slender bodies, using eq 15 to calculate the intrinsic viscosity, one can express the correction constant  $C_2$  in the form

$$C_2 = -1.6 \left( \frac{\lambda^2}{15} \left[ \frac{3}{\ln 2\lambda - 0.5} + \frac{1}{\ln 2\lambda - 1.5} \right] + \frac{8}{5} \right) + \frac{\pi L^3}{16\nu_m^*} \quad (20)$$

In our case, substituting  $L = L_{ef} + d_e = L_{ext} + 0.5$  nm = 41.4 nm,  $\nu_m^* = (\pi/4)d_h^2 L_{ext} = 32.1$  nm<sup>3</sup>,  $[\eta] = 126$ , one obtains, from eq 20,  $C_2 = 232$ . Consequently, for PAA concentration of 250 ppm ( $\Phi_V = 2.5 \times 10^{-4}$ ), the correction to the diffusion coefficient equals  $-5.8\%$ . This is expected to be the maximum correction because the effective length of PAA in electrolyte solutions is much smaller than the extended length  $L_{ext}$ . Obviously, the correction to the hydrodynamic radius is  $5.8\%$ . These values are comparable to experimental error, which suggests that, in the case of PAA of such a low molecular weight, the effect of finite polymer concentration is not too



**Figure 3.** Dependence of the nominal and effective ionization degree of PAA on pH calculated from eqs 25 and 27, for  $pK_a = 4.5$  and  $pK_a = 5.5$  (solid lines 1 and 2, respectively). The full points (circles) denote the experimental results derived from microelectrophoretic measurements.

significant, so the experimental values of  $R_H$  reflect well the infinite dilution situation. Therefore, the discrepancy between theoretical and experimental molecule shape predictions is of a different nature. This can be elucidated in more detail by considering the dynamic viscosity measurements, which are more sensitive to the molecule shape than  $R_H$  values determined by PCS.

Prior to discussion of these results, it is interesting to obtain information on the effective uncompensated charge on PAA molecule under various conditions. Such data can be derived most directly from the electrophoretic mobility  $\mu_e$  measurements. The experimental results are shown in Figure 3 in the form of the dependence of  $\mu_e$  on pH of the PAA solution for various ionic strengths. As can be seen,  $\mu_e$  decreases monotonically with increasing pH and with decreasing ionic strength, attaining the minimum value of  $-2.4 \times 10^{-8} \text{ m}^2(\text{V s})^{-1}$  for  $I = 10^{-3} \text{ M}$  and  $\text{pH} = 9$ . Knowing the mobility, one can calculate the mobile charge on the PAA molecule using the basic electrostatic relationship<sup>28</sup>

$$\mathbf{F} = q\mathbf{E} \quad (21)$$

where  $\mathbf{F}$  is the force acting on the molecule,  $q$  is the effective charge, and  $\mathbf{E}$  is the electric field. Considering that particle velocity due to the force  $\mathbf{F}$  is given by  $\mathbf{U} = \mathbf{M} \cdot \mathbf{F}$ , one can convert eq 21 to the form

$$\mathbf{U} = q\mathbf{M} \cdot \mathbf{E} \quad (22)$$

For uniform electric fields, eq 22 can be simplified to the form

$$q = \frac{\langle U \rangle}{ME} = \frac{kT}{D} \mu_e = 6\pi\eta R_H \mu_e \quad (23)$$

where  $\mu_e$  is the polyelectrolyte mobility,  $\mu_e = \langle U \rangle / E$ , and  $\langle U \rangle$  is the averaged migration velocity of PAA molecules in the uniform electric field  $E$ .

Equation 23 can be directly used for calculations of the averaged number of elementary charges per molecule considering that  $e = 1.602 \times 10^{-19} \text{ C}$ ; thus,

$$N_c = \frac{6\pi\eta}{1.602 \times 10^{-19}} R_H \mu_e \quad (24)$$

Accordingly, the effective ionization degree of the molecule is given by

$$\alpha_i^* = \frac{N_c}{N_m} = \frac{6\pi\eta}{1.602 \times 10^{-19}} \frac{R_H \mu_e}{N_m} \quad (25)$$

where  $N_m$  is the nominal number of charges per molecule.

As shown in ref 31, eq 23 remains valid for spheroids and cylinders if  $2\kappa d_e < 1$ , where  $\kappa^{-1}$  is the electric double layer thickness, given by the expression

$$\kappa^{-1} = \left( \frac{\epsilon kT}{2e^2 I^*} \right) \quad (26)$$

where  $I^*$  is the overall ionic strength of the polyelectrolyte solution, which can be expressed as<sup>12</sup>

$$I^* = \frac{1}{2} \sum z_i^2 n_i + \frac{1}{2} N_c z_c^2 n_p \quad (27)$$

where  $z_i$  is the valency of the ions of the background electrolyte,  $n_i$  is their concentration in the bulk,  $N_c$  is the number of free charges per molecule,  $z_c$  is the valency of the counterions, and  $n_p$  is the concentration of the polyelectrolyte in the solution.

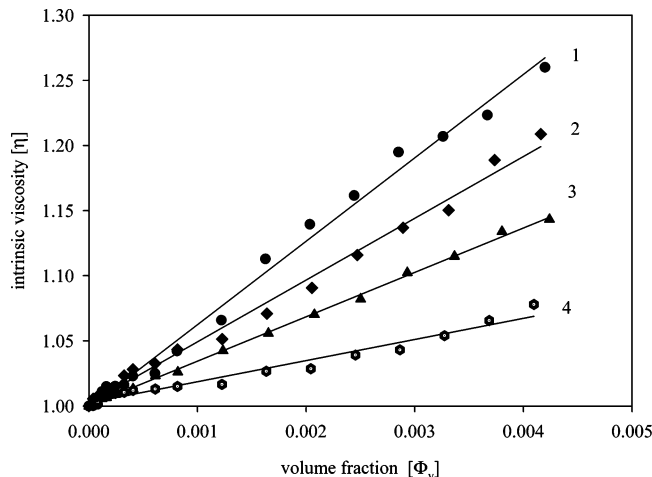
It can be calculated from eq 26 that, for  $T = 293 \text{ K}$  and  $I = 10^{-3} \text{ M}$ ,  $\kappa^{-1} = 9.6 \text{ nm}$ , which gives  $2\kappa d_e = 3.63 \times 10^{-2}$ . For  $I = 0.15 \text{ M}$ ,  $\kappa^{-1} = 0.79 \text{ nm}$ , which gives  $2\kappa d_e = 0.445$ . Because these values are much smaller than unity for the range of ionic strengths used in our measurements, one can expect that eq 23 is fully applicable. Substituting our data, i.e.,  $\mu_e = -2.4 \times 10^{-8} \text{ m}^2(\text{V s})^{-1}$ ,  $R_H = 6.6 \text{ nm}$ ,  $\text{pH} = 9.0$ ,  $I = 10^{-3} \text{ M}$ , one obtains  $N_c = 19$  as the maximum number of free charges (of negative sign) per molecule. This gives the effective ionization degree  $\alpha_i^* = 0.11$  (considering that the nominal number of charges equals 167). For  $I = 0.15 \text{ M}$ ,  $\text{pH} = 9$ ,  $\mu_e = -0.50 \times 10^{-8} \text{ m}^2(\text{V s})^{-1}$ , and  $R_H = 7.9 \text{ nm}$ , which gives  $N = 4.6$  as the maximum number of mobile charges,  $\alpha_i^* = 0.03$ . A similar low ionization degree was predicted for other pH values and ionic strengths. These values are much smaller than the nominal ionization degree of the PAA, which can be calculated from the dependence

$$\alpha_i = \frac{10^{\text{pH} - \text{p}K_a}}{1 + 10^{\text{pH} - \text{p}K_a}} \quad (28)$$

where the  $\text{p}K_a$  value for PAA is reported to lie between 4.5<sup>32</sup> and 6.5<sup>33</sup>

It can be calculated from eq 28 that, for  $\text{pH} = 9$ , the nominal ionization degree equals 1 for  $\text{p}K_a = 4.5$ – $6.5$ . For  $\text{pH} = 4$ , one obtains  $\alpha_i = 0.24$  for  $\text{p}K_a = 4.5$ . The nominal ionization degree derived from eq 28 is compared in Figure 3 with experimental data derived from microelectrophoresis ( $\alpha_i^*$  calculated from eq 25). The large deviation of experimental data from theoretical predictions calculated from eq 28 indicates unequivocally that the molecule charge is compensated to a large extent by specific adsorption of counterions ( $\text{Na}^+$  in our case). This behavior is often referred to as the ion condensation phenomenon<sup>12,18</sup>. Similar behavior was reported by Plucktaveesak et al.,<sup>13</sup> who determined the effective ionization degree of PAA using the ion-selective electrode sensitive to the sodium ions. However, the values reported in their work, varying between 0.23 and 0.14, were higher than our data determined under similar experimental conditions. A possible source of this difference is the higher molecular weight of the PAA sample (90 kD) and the limited precision of the indirect measurements done with





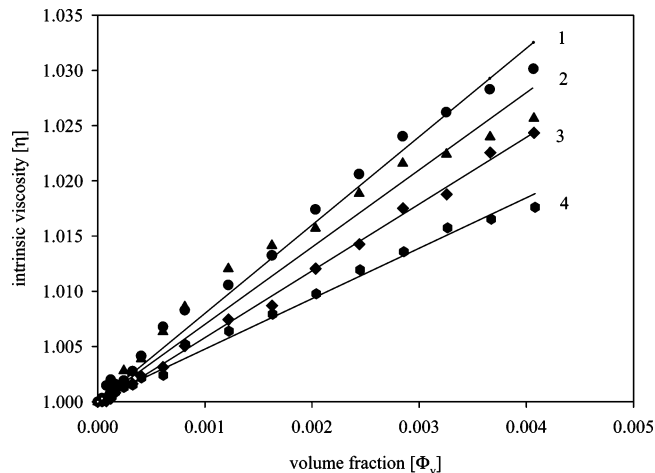
**Figure 4.** Dependence of the intrinsic viscosity  $\eta_s/\eta_{\text{water}}$  of PAA volume fraction  $\Phi_v$ ,  $T = 293$  K,  $\text{pH} = 9.0$ ,  $\alpha = 1$ ,  $\alpha^* = 0.085$ , (1)  $I = 10^{-3}$  M, (2)  $I = 5 \times 10^{-3}$  M, (3)  $I = 10^{-2}$  M, (4)  $I = 0.15$  M.

the ion-selective electrode (measured free sodium ions in solution), especially in the range of lower pH.

It is interesting to compare our experimental data with the effective ionization degree derived from simulations. It was found that, for the nominal ionization degree of 1 (167 charges per molecule initially), the final (equilibrium) number of uncompensated charges was 42, which gives the ionization degree of 0.25 for the ionic strength of  $10^{-3}$  M. Analogously, for the ionic strength of 0.15 M, the ionization degree found in simulations was 0.17. As can be noticed, this is significantly higher than our experimental data obtained for  $\text{pH} = 9$ . For the nominal ionization degree  $\alpha_i^* = 0.5$ , it was predicted theoretically that the effective ionization degree  $\alpha$  varied between 0.15 and 0.1. This deviation seems to appear because, in the theoretical simulations, the ion hydration effects as well as variations in the dielectric constant at small distances between ion pairs were neglected. It is usually assumed that the value of the dielectric constant of water decreases to 5–10, for distances below 1 nm. This will appreciably increase the energy of ion-pair formation, leading to a decrease in the effective charge of PAA.

It seems that this hypothesis can be verified by exploiting the intrinsic viscosity measurements, which are more sensitive to the effective length of the molecule than the hydrodynamic radius measurements. The intrinsic viscosity was determined from the slope of the dependence of the reduced dynamic viscosity  $\eta_s/\eta$  on the polyelectrolyte volume fraction  $\Phi_v$ . Examples of such measurements for various ionic strengths,  $\text{pH} = 9$  and 4, are shown in Figures 4 and 5. As can be seen, in all cases, the dependence of  $\eta_s/\eta$  on  $\Phi_v$  can be fitted well by the straight lines with the slope decreasing systematically with ionic strength. It was determined that, for  $I = 10^{-3}$  M,  $\text{pH} = 9$  and  $\eta_s/\eta = 63$ , and for  $I = 0.15$  M,  $\text{pH} = 9$  and  $\eta_s/\eta = 17$  (for sake of convenience, the experimental values of the intrinsic viscosity are compiled in Table 4). As can be deduced, these values are much larger than the theoretical slope for spheres, equal to 2.5. To some extent, this deviation can be explained by the hydration of the molecule, which increases its apparent size in the solution and, consequently, its volume fraction.<sup>22</sup> The significance of this effect can be estimated by considering that the effective volume of the PAA molecule equals

$$v_m^* = v_m \left( \frac{d_c}{d_h} \right)^2 = 2v_m$$



**Figure 5.** Dependence of the intrinsic viscosity  $[\eta]$  of PAA on the volume fraction  $\Phi_v$ ,  $T = 293$  K,  $\text{pH} = 4.0$ ,  $\alpha = 0.22$ ,  $\alpha^* = 0.022$ , (1)  $I = 10^{-3}$  M, (2)  $I = 5 \times 10^{-3}$  M, (3)  $I = 10^{-2}$  M, (4)  $I = 0.15$  M.

**TABLE 4: Experimental Values of the Intrinsic Viscosity  $[\eta]$ , the Corrected Viscosity  $[\eta]_c$ , the Equivalent Aspect Ratio  $\lambda_c$ , and the Equivalent Rod Length  $L_{\text{ef}}$ <sup>a</sup>**

pH ionization degree		ionic strength [M]			
		$10^{-3}$	$5 \times 10^{-3}$	$10^{-2}$	0.15
pH = 9, $\alpha = 1$	$\kappa^{-1}$ [nm]	9.6	4.29	3.03	0.78
	$[\eta]$	63.0	48.0	34.0	17.0
	$[\eta]_c$	32.0	24.0	17.0	8.5
	$\lambda_c$	18.0	14.5	11.6	7.0
	$L_{\text{ef}}$	23.5	20.5	17.6	12.5
	$L_{\text{ef}}$ theory	21.0		18.5	10.5
pH = 5.5, $\alpha = 0.5$	$[\eta]$	22.0	19.0	17.0	14.0
	$[\eta]_c$	11.0	9.5	8.5	7.0
	$\lambda_c$	8.5	7.7	7.0	5.9
	$L_{\text{ef}}$	14.3	13.4	12.6	11.2
pH = 4.0, $\alpha = 0.2$	$[\eta]$	8.0	7.0	5.9	4.6
	$[\eta]_c$	4.0	3.5	3.0	2.3

<sup>a</sup>  $[\eta]_c = 0.5[\eta]$  corrected for hydration,  $L_{\text{ef}} = (4\nu^*\lambda_v^2/\pi)^{1/3}$ .

Accordingly, the effective volume fraction of the polymer should be increased by the factor of 2; consequently, the effective intrinsic viscosity is reduced by the same factor. The corrected viscosity data are also shown in Table 4. It is interesting to observe that the corrected values of the intrinsic viscosity for  $\text{pH} = 9$  decrease with the ionic strength proportionally to  $I^{-1/3}$ . This agrees quite well with the experimental results of Davis and Russel<sup>19</sup> obtained for potassium poly(styrene sulfonate) having a quite similar extended length of 49.4 and chain diameter of 1 nm. Their experimental data were successfully interpreted in terms of the Yamakawa model predictions with the correction for the volume excluded effect.

On the other hand, for  $\text{pH} = 4$  and the ionic strength of 0.15 M, the corrected viscosity value found experimentally was 2.3, which is quite close to the theoretical value predicted for spheres from the Einstein model. This behavior was not observed by Davis and Russel,<sup>19</sup> however, who measured the intrinsic viscosity values of 9, even at the ionic strength of 1 M. This discrepancy can be attributed partially to the hydration effect, which was not considered by these authors and to the higher stiffness of the poly(styrene sulfonate) chain.

Except for the increase in the particle volume, it is often suggested that the intrinsic viscosity is increased because of the primary electroviscous effect, consisting of deformation of electrical double layers under shearing flows. The correction to the intrinsic viscosity of suspensions due to the primary

electroviscous effect can be calculated from the formula<sup>29,34</sup>

$$p = \frac{\epsilon \zeta^2 (1 + \kappa a)^2 F_e(\kappa a)}{\eta D_i} \quad (29)$$

where  $a$  is the characteristic dimension of the molecule,  $\zeta$  is the zeta potential of the polymer calculated from the electrophoretic mobility by assuming the Henry model of electrophoretic motion,  $D_i$  is the characteristic diffusion coefficient of the electrolyte ions, and  $F_e$  is the dimensionless function given in ref 34. By substituting our experimental data ( $I = 10^{-3}$  M,  $a = 10$  nm,  $\kappa a = 0.11$ ,  $F_e(1 + \kappa a)^2 = 0.1$ , and  $\zeta = -50$  mV), one obtains from eq 28  $p = 0.0885$ . Since this value is much smaller than unity, one can assume that the significance of the electroviscous effect is negligible for our experimental conditions.

Hence, it seems justified to attribute the high values of the intrinsic viscosity of PAA to the elongated shape of the molecule. This can be quantitatively accounted for by the hydrodynamic model discussed above, which is valid for flows characterized by  $Pe \ll 1$ . This inequality was fulfilled in our case for PAA viscosity measurements because the averaged shear rate  $\langle G \rangle$  was  $1.8 \times 10^2 \text{ s}^{-1}$  and the rotary diffusion  $D_{r_h} = 2.2 \times 10^5 \text{ s}^{-1}$  (see Table 3). This gives  $Pe = 8.2 \times 10^{-4}$ , which justifies the use of eqs 13–15 resulting from Brenner's hydrodynamic theory for interpreting the intrinsic viscosity data. Assuming that the shape of the molecule can be approximated by a prolate spheroid, one can calculate, by numerically inverting eq 13, the dimensionless aspect ratio parameter  $\lambda_c$  (longer-to-shorter axis ratio of the equivalent spheroid). Values of  $\lambda_c$  calculated in this way are collected in Table 4. As can be seen, for pH = 9, the aspect ratio varies between 18 (for  $I = 10^{-3}$  M) and 7 (for  $I = 0.15$  M). By taking the hydrated chain diameter  $d_h = 1$  nm, one can calculate that this corresponds to the equivalent length of the molecule varying between 23.5 and 12.5 nm (for  $I$  changed between  $10^{-3}$  and 0.15 M). This correlates well with theoretical predictions, i.e., 21–10.5 nm, derived for the same range of ionic strength. However, for lower pH (corresponding to much lower ionization degree), calculations of the equivalent length of the molecule from the  $\lambda_c$  parameter are not feasible because of the ambiguity in properly defining the molecule shape.

Nevertheless, it can be deduced that the experimental results collected in Table 4 are in good agreement with theoretical simulations, predicting a significant folding of PAA for pH = 4 and higher ionic strength. However, the PCS hydrodynamic radius measurements exclude the possibility of forming a compact structure of a spherical shape upon folding. This is so because the experimentally determined value of  $R_H$  for pH = 4 and  $I = 0.15$  was 5.8 nm instead of 1.72 nm predicted for the sphere having the same hydrated volume as the stretched PAA molecule. This paradox can be resolved by postulating that, because of significant hydration, the PAA molecule forms upon folding a helicoidal structure rather than a sphere or a oblate spheroid (a compact disk). However, the limited accuracy of the measurements and lack of hydrodynamic theories of resistance coefficient and intrinsic viscosity for such complicated structures prohibits more quantitative considerations.

It is interesting to mention that our intrinsic viscosity measurements for high ionization degree were roughly proportional to  $I^{-1/3}$ , which is in agreement with the theoretical slope predicted by the Yamakawa model with the correction for the volume excluded effect introduced by Davis and Russel.<sup>19</sup>

## IV. Concluding Remarks

The structure of PAA molecules in electrolyte solutions can be predicted to a significant extent by molecular dynamic simulations. Numerical calculations suggest that, for not too high ionic strength, the molecule assumes the shape of a flexible rod with the effective length decreasing with increased ionic strength and ionization degree. It was predicted theoretically that the effective ionization degree of the molecule for pH = 9 varied between 0.25 and 0.17 for the ionic strength changing between  $10^{-3}$  and 0.15 M. Measurements of the electrophoretic migration velocity of PAA confirmed this prediction, although the experimental ionization degree was found to be even lower, varying between 0.11 and 0.03, for the same conditions. These low values of ionization degree, decreasing with ionic strength, were accounted for by counterion adsorption on the PAA molecule, often referred to as the ion condensation effect.

On the basis of the molecule shape predictions, the hydrodynamic model was formulated postulating a fast relaxation of local flow in comparison with the diffusion relaxation time of the molecule position. The hydrodynamic radius calculated from this model by exploiting the resistance coefficient of spheroids, either stretched or bent to various forms, was in agreement with experimental data derived from PCS. This hydrodynamic model was also applied for interpretation of the dynamic viscosity measurements. It was found that the measured intrinsic viscosity data for pH = 9 corrected for the chain hydration effect were well accounted for by Brenner's theory for prolate spheroids. The equivalent length of these spheroids correlated well with the effective length of PAA molecule derived from numerical simulations.

Discrepancies between experimental data and theoretical predictions occurred for low ionization degree and higher ionic strength. From simulation, a significant folding of the molecule to the form of a sphere was predicted, whereas this was not confirmed by the hydrodynamic radius measurements. This deviation probably appeared because the hydration of the PAA molecule was neglected in numerical simulations.

The most probable shape of PAA for low ionic strength is a flexible rod bent to the form of a semicircle or a torus, and for high ionic strength (lower ionization degree), it is bent to the form of a helicoidal structure.

**Acknowledgment.** This work was partially supported by EC Grant "NANOCAPS" NMP4-CT-2003-001.

## References and Notes

- (1) Decher, G.; Honig, J. D.; Schmitt, J. *Thin Solid Films* **1992**, 831, 210.
- (2) Lvov, Y. M.; Decher, G.; Möhwald, H. *Langmuir* **1993**, 9, 481.
- (3) Decher, G. *Science* **1992**, 277, 1232.
- (4) Lvov, Y. M.; Ariga, K.; Onda, M.; Ichinose, I.; Kunitake, T. *Colloids Surf., A* **1999**, 146, 337.
- (5) Hammond, P. T. *Curr. Opin. Colloid Interface Sci.* **2000**, 4, 430.
- (6) Lvov, Y. M. Polyion-Protein Nanocomposite films. In *Encyclopedia of Surface and Colloid Science*; Hubbard, A. T., Ed.; Marcel Dekker: New York, 2002; Chapter 3, p 4162.
- (7) Fuoss, R. M. *Discuss. Faraday. Soc.* **1951**, 11, 125.
- (8) Cohen, J.; Priel, Z. *J. Chem. Phys.* **1988**, 88, 711.
- (9) Yamanaka, J.; Matsuoka, H.; Kitano, H.; Hasegawa, M.; Ise, N. *J. Am. Chem. Soc.* **1990**, 112, 587.
- (10) Boris, D. C.; Colby, R. H. *Macromolecules* **1998**, 31, 5746.
- (11) Jiang, L.; Yang, D.; Chen, S. B. *Macromolecules* **2001**, 34, 3730.
- (12) Rushing, T. S.; Hester, R. D. *Polymer* **2004**, 45, 6587.
- (13) Plucktaueesak, N.; Konop, A. J.; Colby, R. H. *J. Phys. Chem. B* **2003**, 107, 8166.
- (14) deGennes, P. G.; Pincus, P.; Velasco, R. M.; Brochard, F. *J. Phys.* **1976**, 37, 1461.
- (15) Odjik, T. *J. Polym. Sci., Polym. Phys. Ed.* **1997**, 15, 477.
- (16) Skolnick, J.; Fixman, M. *Macromolecules* **1977**, 10, 944.

- (17) Davis, R. M.; Russel, W. B. *Macromolecules* **1987**, *20*, 518.  
(18) Yamakawa, A.; Fujii, M. *Macromolecules* **1974**, *7*, 128.  
(19) Davis, R. M.; Russel, W. B. *Macromolecules* **1987**, *20*, 518.  
(20) Kirkwood, J. G.; Auer, P. L. *J. Chem. Phys.* **1951**, *19*, 281.  
(21) Brenner, H. *J. Multiphase Flow* **1974**, *1*, 195.  
(22) Harding, S. E. *Biophys. Chem.* **1995**, *55*, 69.  
(23) *HYPERCHEM*, version 7.5; HyperCube Inc.: Gainesville, FL.  
(24) Cornell, W. D.; Cieplak, P.; Bayly, C. I.; Gould, I. R.; Merz, K. M., Jr.; Ferguson, D. M.; Spellmayer, D. C.; Fox, T.; Caldwell, J. W.; Kollman, P. A. *J. Am. Chem. Soc.* **1995**, *117*, 5179.  
(25) Gasteiger, J.; Marsili, M. *Tetrahedron* **1980**, *36*, 3219.  
(26) Chodanowski, P.; Stoll, S. *J. Chem. Phys.* **1999**, *111*, 6069.  
(27) Adamczyk, Z.; Zembala, M.; Warszyński, P.; Jachimska, B. *Langmuir* **2004**, *20*, 10517.  
(28) Adamczyk, Z. *Particles at Interfaces: Interactions, Deposition, Structure*; Elsevier: New York, 2006.  
(29) van De Ven, T. G. M. *Colloidal Hydrodynamics*; Academic Press: New York, 1989.  
(30) Russel, W. B.; Saville, D. A.; Schowalter, W. R. *Colloidal Dispersions*; Cambridge University Press: New York, 1991.  
(31) Yoon, B. J.; Kim, S. *J. Colloid Interface Sci.* **1989**, *128*, 275.  
(32) Pokrel, M. R.; Bossmann, S. H. *J. Phys. Chem.* **2000**, *104*, 2215.  
(33) Choi, J.; Rubner, M. F. *Macromolecules* **2005**, *38*, 116.  
(34) Laven, J.; Stein, H. N. *J. Colloid Interface Sci.* **2001**, *238*, 8.